Magn. Reson., 5, 143–152, 2024
https://doi.org/10.5194/mr-5-143-2024

Open Access
MAGNETIC RESONANCE

Design and performance of an oversized-sample 35 GHz EPR resonator with an elevated Q value

Jörg Wolfgang Anselm Fischer[1,★], Julian Stropp[1,★], René Tschaggelar[1,★], Oliver Oberhänsli[1], Nicholas Alaniva[1], Mariko Inoue[2], Kazushi Mashima[2], Alexander Benjamin Barnes[1], Gunnar Jeschke[1], and Daniel Klose[1]

[1]Institute for Molecular Physical Science, ETH Zurich, Vladimir-Prelog-Weg 2, 8093 Zurich, Switzerland
[2]Department of Chemistry Graduate School of Engineering Science, Osaka University,
1–3 Machikaneyama-cho, Toyonaka, Osaka 560-8531, Japan
★These authors contributed equally to this work.

Correspondence: Daniel Klose (daniel.klose@phys.chem.ethz.ch)

Received: 29 April 2024 – Discussion started: 7 May 2024
Revised: 4 July 2024 – Accepted: 3 August 2024 – Published: 20 September 2024

Abstract. Continuous-wave electron paramagnetic resonance (EPR) spectroscopy at 35 GHz is an essential cornerstone in multi-frequency EPR studies and is crucial for differentiating multiple species in complex systems due to the improved g-tensor resolution compared to lower microwave frequencies. Especially for unstable and highly sensitive paramagnetic centers, the reliability of the measurements can be improved upon through the use of a single sample for EPR experiments at all frequencies. Besides the advantages, the lack of common availability of oversized-sample resonators at 35 GHz often limits scientists to lower frequencies or smaller sample geometries, and the latter may be non-trivial for sensitive materials. In this work, we present the design and performance of an oversized-sample 35 GHz EPR resonator with a high loaded Q value, Q_L, of up to 2550, well-suited for continuous-wave EPR and pulsed single-microwave-frequency experiments. The design is driven by electromagnetic field simulations, and the microwave characteristics of manufactured prototypes were found to be in agreement with the predictions. The resonator is based on a cylindrical cavity with a TE_{011} mode, allowing for 3 mm sample access. The design targets that we met include high sensitivity, robustness, and ease of manufacturing and maintenance. The resonator is compatible with commercial EPR spectrometers and with helium flow, as well as with cryogen-free cryostats, allowing for measurements at temperatures down to 1.8 K. To highlight the general applicability, the resonator was tested on metal centers, as well as on organic radicals featuring extremely narrow lines.

1 Introduction

Electron paramagnetic resonance (EPR) spectroscopy is a versatile and sensitive technique ideally suited to probe paramagnetic centers, even in complex environments such as heterogeneous catalysts (Bonke et al., 2021). Chemical and structural information on the paramagnetic center is encoded in parameters of the effective spin Hamiltonian, describing the unpaired electron spin(s), as well as coupled magnetic nuclei (Roessler and Salvadori, 2018; Schweiger and Jeschke, 2001). For systems with a single electron spin ($S = 1/2$), the solid-state continuous-wave (CW) EPR spectra measured at the common frequency of 9.5 GHz (i.e., X band) are dominated by the anisotropic Zeeman interaction and the anisotropic hyperfine interaction described by the g tensor and the A tensor, respectively. For the case of significant g and A anisotropy, as found in transition metal complexes, spectra can be several gigahertz wide. Accordingly, for many applications, a high sensitivity is essential. Key determining factors for the sensitivity of an EPR spectrometer are the resonator properties, including the sample volume it allows.

In addition to sufficient sensitivity, resolution and spectral overlap are of concern for the analysis of complex samples,

such as heterogeneous catalysts, where several paramagnetic species may be present. Already for a single anisotropic paramagnetic species, the number of parameters in the spin Hamiltonian is regularly beyond what can be resolved in a single CW EPR spectrum (NejatyJahromy et al., 2021). The presence of several paramagnetic species often leads to severe spectral overlap, which occludes access to the full information on each individual species inherent in the CW EPR line shape. To alleviate this challenge, multi-frequency EPR is employed as an essential tool to deconvolute overlapping spectral components and to constrain the full set of the anisotropic interactions in the spin Hamiltonian (Misra, 2011). Multi-frequency EPR typically makes use of a combination of frequencies and corresponding magnetic field ranges, with the most accessible frequencies being ~ 4 GHz (S band), ~ 9.5 GHz (X band), ~ 35 GHz (Q band), and ~ 95 GHz (W band). This serves, first, to disentangle the field-dependent Zeeman interaction and the field-independent hyperfine interaction and, second, to increase the spectral resolution for the g tensor at higher fields. This approach is known to aid in the differentiation of multiple spectral species (Misra, 2011). For samples with (residual) motion of the paramagnetic centers, the different frequencies are sensitive to different motional averaging time windows; hence, multi-frequency EPR can also enhance studies of the inherent dynamics (Zhang et al., 2010).

An important concern for global analysis of multi-frequency EPR data is the line shape of the spectra when obtained with either CW or pulsed EPR excitation. Pulsed EPR acquires spectra via detection of an electron spin echo or a free induction decay (FID) and can be sensitive towards broad signals with small slopes in the absorption spectrum. Yet, typically, pulsed EPR has a reduced line shape fidelity or sensitivity compared to CW EPR experiments for two main reasons. First, using high microwave power for pulse excitation leads to instrumental dead time due to the need for transient receiver protection. This dead time can, however, make up a significant fraction of the transverse relaxation time, leading to signal loss, which is especially troublesome in cases where the relaxation is anisotropic across the spectrum. Second, electron spin echo envelope modulation (ESEEM) due to nuclear hyperfine interactions exhibits a magnetic-field-dependent initial phase and may thus lead to distortions of the absorption spectrum unless long interpulse delays are used. Due to these considerations, the observed relative intensities of different species and also those within a single spectral species may differ between CW and pulsed EPR spectra, yet only the CW EPR line shape in the absence of microwave power saturation is insensitive to relaxation time differences.

For samples of limited stability, such as catalysts that are highly sensitive to oxygen or moisture, or for samples that are challenging to reproduce quantitatively, such as ex situ freeze-trapped reaction intermediates, it is highly advantageous to record multi-frequency EPR data on the very same sample. This requires resonators that allow for the same sample tube diameter at different microwave frequencies (Tschaggelar et al., 2009) and is particularly important for a quantitative global analysis by spectral simulations (Stoll and Schweiger, 2006), where variations in the relative contributions of different species between the spectra taken at different frequencies cannot be tolerated. With sample dimensions in EPR spectroscopy being comparable to the wavelength, at least at the higher frequencies, the requirement to measure the same sample at different frequencies poses a technical challenge. Sensitivity optimization requires larger sample volumes at lower frequencies (Misra, 2011), with typical sample tube outer diameters (ODs) of 5 mm at S-band frequencies and of 4 mm at X-band frequencies. However, even an OD of 3 mm already exceeds a quarter of the wavelength at Q-band frequencies and corresponds to the approximate wavelength at W-band frequencies. When we consider a 3 mm OD sample tube as a reasonable compromise, the sample is thus *oversized* at Q- and W-band frequencies. Therefore, the properties of the resonant cavity are strongly influenced by the dielectric properties of the sample tube and the sample. This poses a challenge for the design of a robust cavity resonator, particularly for CW EPR, where adequate sensitivity requires a high quality (Q) factor.

For Q-band frequencies of about 33–36 GHz, different types of resonators have been designed and evaluated. Loop-gap resonators, originally introduced by Froncisz and Hyde (1982), are well-suited to concentrate the microwave B_1 field to a limited sample volume. Several designs of Q-band loop-gap resonators have been published (Mett et al., 2009; Forrer et al., 2008; Denysenkov et al., 2017), and B_1 fields corresponding to a Rabi frequency of 40 MHz over bandwidths > 1 GHz have been achieved (Tschaggelar et al., 2017). However, scaling to larger sample diameters strongly deteriorates the performance of loop-gap resonators. Also, for high-B_1 and large-bandwidth pulsed EPR applications, a cylindrical resonator operating with the TE_{011} mode was computed for an oversized sample with 3 mm OD, whereas the actual resonator used a central dielectric ring for enhancing the B_1 field for a smaller sample OD of 1.8 mm (Raitsimring et al., 2012). For the 3 mm OD sample access that we are aiming for here, cubic box resonators in TE_{102} mode (Tschaggelar et al., 2009; Polyhach et al., 2012) and cylindrical cavity resonators in TE_{011} mode (Reijerse et al., 2012; Judd et al., 2022; Savitsky et al., 2013; Gromov et al., 2006; Sienkiewicz et al., 1996) have been developed for different applications. Among these, the cylindrical cavities feature a higher Q factor, as well as a better conversion factor, and the larger sample volumes overcompensate for their poorer filling factors compared to commercial dielectric resonators (Reijerse and Savitsky, 2017).

Here, based on the design target of a high-Q Q-band resonator for oversized samples suitable for CW EPR with high sensitivity, we report on the design and performance of a robust, simple cylindrical TE_{011}-mode cavity resonator for

3 mm OD sample tubes. While suitable primarily for sensitive CW EPR experiments, the resonator can be also used for pulsed single-microwave-frequency experiments, particularly if a long receiver protection, and hence spectrometer dead time, can be tolerated. The resonator design is based on electromagnetic field modeling by finite-element calculations in order to minimize the effect of electric fields in the sample and to optimize the Q factor. The experimentally determined characteristics are in good agreement with the calculated properties, highlighting the advantage of a design approach based on electromagnetic field simulations. The resonator performance was tested on a scope of samples including a homogeneous, multi-component Ti(III) catalyst in toluene under cryogenic conditions and at room temperature to demonstrate the general applicability. The linewidth resolution was demonstrated with an N@C_{60} sample to be better than 10^{-2} mT.

2 Materials and methods

2.1 Finite-element simulations of electromagnetic structures

Electric field and magnetic field calculations were carried out by finite-element simulations with the software CST Microwave Studio (CST GmbH, Darmstadt, Germany), which uses a volume grid discretization. The geometric structure was modeled in silico, with all parts of the resonator in contact with the microwave fields. Out-of-resonance losses were fitted by assigning a surface conductivity of 3×10^4 S m^{-1} to the waveguide and other (non-ideal) surfaces. All metal structures were calculated using a surface impedance model to incorporate resistive losses. The geometry of the resonator has been parameterized and optimized in terms of center frequency, bandwidth, B_1 field strength, sample volume (filling height of a sample tube with 3.0 mm OD, 2.2 mm inner diameter (ID)), and coupler position for different sample materials (with relative dielectric constants ranging from 1 for empty tubes up to 3 for frozen aqueous samples; Matzler and Wegmuller, 1987). The frequency shift of the resonator upon introduction of the sample tube could be reproduced using a relative permittivity of 3.4 for the quartz sample tube at Q-band frequencies.

Simulations of the input reflection coefficient S_{11} were used to describe the measured microwave reflection curves. For comparison with the experimental results obtained on a point sample, the microwave field and frequency were simulated at specific locations within the resonator, excluding losses and surface imperfections.

2.2 Microwave reflection curves and resonator characterization

The experimental microwave reflection curves were measured as the scattering parameter S_{11} with a calibrated network analyzer (HP 8722ES) and a source power of −10 dBm at room temperature. The simulated microwave reflection curves with the input reflection coefficient S_{11} were obtained from finite-element simulations as described above. Details on the calculation of the β parameter and the half-power points ($\nu_{\mathrm{hp},i}$) for the Q value calculation and the filling factor η are given in Sects. S1, S2, and in Fig. S1 in the Supplement.

2.3 Prototype fabrication

The resonator cavity, including the iris, was fabricated from a solid block of copper metal (purity 99.95 %, ThyssenKrupp, Essen, Germany) by wire erosion to yield suitably smooth surfaces. The iris groove was cut from the outside by CNC milling, with the coupling rod (1 mm, copper) positioned between the iris and WR28 waveguide (copper, Penn Engineering Components, Valencia, USA). The modulation coils consist of 30 turns of lacquer-isolated copper wire with a diameter of 0.35 mm. The coils were wound in a rectangular arrangement with a height of 20 mm and a width of 15 mm, and they were mounted at a distance of 25 mm. With an induction of 350 µH, a root-mean-square (rms) current of 250 mA is required for a modulation amplitude of 0.1 mT.

2.4 Sample preparation

Diphenyl-1-picrylhydrazyl (DPPH, Sigma, Buchs, Switzerland) radical powder, N@C_{60} (powder, 6.15 mg, 10 ppm spin-diluted with C_{60}, Designer Carbon Materials Ltd., Oxford, UK) (Franco et al., 2006; Eckardt et al., 2015; Jakes et al., 2003), or 20 µL, 100 µM (4-Hydroxy-2,2,6,6-tetramethylpiperidine-1-oxyl – TEMPOL) radical solution in toluene were filled into 3.0 mm OD (ca. 2.4 mm ID) sample tubes made from Heraeus HSQ300 electrically fused quartz (Aachener Quarzglas, Aachen, Germany). The Herasil sample was a cylinder with a height of 6 mm and a diameter of 2.4 mm that was γ-irradiated with a dose of 2 kGy. The titanium catalyst in toluene solution was prepared in a glove box under Ar atmosphere by using a Ti(IV) organometallic precursor reduced to Ti(III) by trimethylaluminum; details will be described elsewhere. The filling height for the samples was ca. 8 mm, except for Herasil, TEMPOL, and DPPH; the latter was prepared using a small visible amount to approximate a point sample.

2.5 EPR measurements

Room-temperature CW EPR experiments, as well as the nutation measurements by pulsed EPR, were performed on a home-built pulse/CW Q-band EPR spectrometer equipped with a helium flow cryostat (CF935, Oxford Instruments, Oxfordshire, UK) and a traveling wave tube amplifier (nominal power of 150 W) described by (Gromov et al., 2001). For experiments at room temperature, the temperature of the resonator was maintained by a gentle flow of dry nitrogen

gas through the cryostat. For DPPH, a microwave power of 0.32 µW, a lock-in time constant of 20.48 ms, and a conversion time of 81.92 ms were used; the modulation frequency was set to 100 kHz; and the modulation amplitude was set to 0.02 mT. The Rabi nutation experiment was performed using a $t_p - T - \pi/2 - \tau - \pi - \tau -$ echo pulse sequence, and the input power into the resonator during the pulses was subsequently measured at the microwave bridge output with a 437B RF power meter (Keysight). The CW EPR spectra of the titanium catalyst and for N@C_{60} were measured on a commercial EPR spectrometer (ELEXSYS E580, Bruker Biospin, Rheinstetten, Germany), equipped with a cryogen-free variable-temperature EPR cryostat (Cryogenic Ltd., London, UK). The Ti(III) spectra were recorded without over-modulation with a modulation frequency of 100 kHz. At room temperature, 0.1 mT modulation amplitude, 161.84 ms conversion time, and 0.57 µW microwave power were used, while at 30 K, the settings were 0.1 mT, 81.92 ms, and 0.23 µW, respectively. The N@C_{60} was measured at room temperature, with a modulation frequency of 100 kHz and a modulation amplitude of 0.002 mT. A microwave power of 0.23 µW and a conversion time of 160 ms were used. CW EPR parameters were chosen for optimal signal-to-noise ratios while avoiding power saturation of the samples, as well as saturation of the receiver chain of the spectrometer. An overview of all measurement parameters can be found in Table S1 in the Supplement.

3 Results and discussion

3.1 Resonator design

The Q-band resonator is designed for sample tubes up to 3 mm OD and a temperature range from 1.8 to 298 K in continuous He flow cryostats or cryogen-free systems. Special focus was placed on low losses for a high Q factor, suitability for applications with different solvents, repeatable manufacturability, robust design, and easy handling and cleaning. This is achieved by a cylindrical TE_{011} cavity (9 mm height, 11.5 mm diameter) in a copper block with modulation coils from copper wire that are mounted on both outer sides of the cavity block (Fig. 1a). The modulation field at the sample position for a given current in the modulation coils is enhanced by horizontal slots in the copper block dissecting the entire length of the lateral walls (Fig. 1a). Electromagnetic field simulations have been performed by systematically varying the slot size for the resonator between 0.2 and 0.8 mm in 0.5 mm steps. The resulting S_{11} curves (Fig. S2) exhibit a minimum of the dip around 0.5 mm, which was hence chosen to manufacture the resonator. While in this optimization approach the modulation field is not calculated, a more involved approach such as that performed by Sidabras et al. (2017) might further improve the performance of the resonator.

The cavity height-to-diameter ratio was optimized for minimum reflection (dip depth) at a frequency around 34.2 GHz with an empty sample tube. The obtained geometry (9 mm × 11.5 mm; see Table S2) is close to, yet not the same as, that of the TE_{011} resonator designed by Reijerse et al. (2012). The deviation from the expected optimum with a ratio of 1 : 1 may arise due to the interaction of the electromagnetic fields with the oversized sample. With the optimized cavity height-to-diameter ratio, unwanted modes are suppressed or shifted out of the targeted frequency range. In case of sample damage in the cavity, the removable bottom plate of the resonator allows for efficient cleaning. The microwave power is provided through a waveguide, made from copper in the bottom part and from stainless steel in the upper part to reduce thermal conductivity. The coupling of the microwave from the waveguide into the cavity is adjusted by a copper coupler in front of the iris (0.5 × 3.0 mm with rounded ends). Rotating the coupling knob at the top flange of the probe head tilts the coupler by some degrees from the vertical position and thereby changes the coupling. This is achieved by a thread just above the cavity, which converts the rotation into a tilt. The 3 mm OD sample tube held by the tip of a sample tube holder is guided in a 8 mm Vetronite tube from the top flange to the resonator at its bottom. For precise and reproducible positioning, the sample tube is inserted through a conical guide into the center of the cavity.

3.2 Simulations and experimental characterization of the resonator

The electromagnetic field configurations in the cavity were simulated and are depicted in Fig. 1b–e. Figure 1b and c show horizontal and vertical cross sections through the cavity, with the simulated x component of the magnetic field B_1 of the incident microwaves. Since the x component of B_1 is orthogonal to the horizontal external magnetic field B_0 along z, the excitation of electron spins depends linearly on its strength. In Fig. 1, the space between the isolines corresponds to 6 % steps of the maximum field strength. Vertically, within ±2 mm around the position with the maximum B_1 field strength, the field decays to about 80 %. The horizontal, radial decay of B_1 inside the sample (2.2 mm inner diameter) is below 10 % and, therefore, is negligible compared to the vertical decay. Spins which are located outside the vertical center region will experience a lower B_1 field and hence will contribute to a smaller extent to the EPR signal. This is verified experimentally by the measurement of a point sample at different vertical positions in the resonator (Fig. 2). The magnetic field strength and its distribution showed only slight changes for samples with different dielectric constants. Observing the magnetic vector field across the range of conditions that we target with the present design, we found that the phase of the magnetic field remains constant over the volume of the sample, an example of which is shown in Fig. S3.

The electric field distribution of the TE_{011} mode is shown in Fig. 1d and e. The cavity is designed such that the electric field in the sample volume is minimized to avoid sample

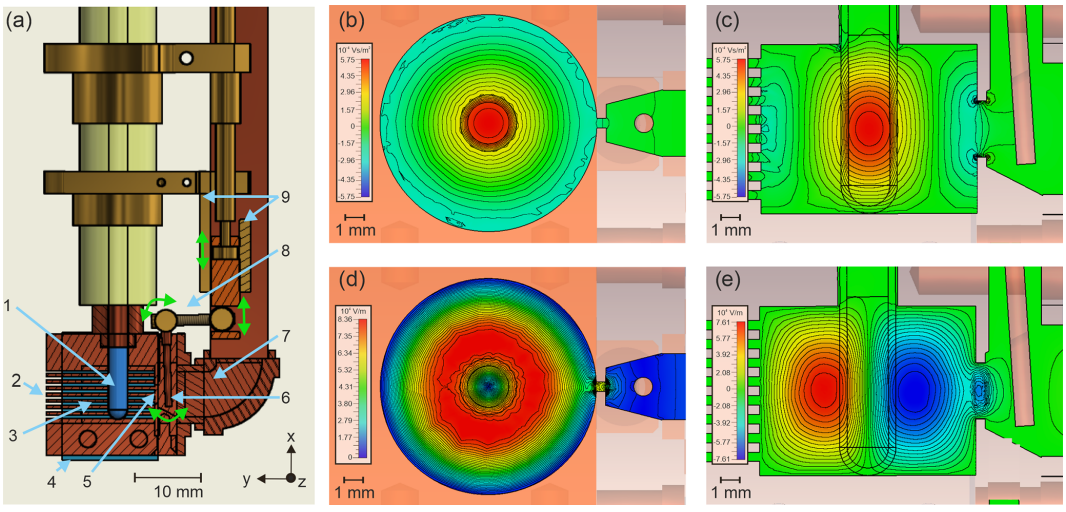

Figure 1. **(a)** Rendering of the Q-band EPR resonator with a cross section view of certain parts to show the technical functionality: EPR tube (1), slits for modulation field (2), cavity (3), modulation coil holder (4), iris (5), coupler (6), coupling waveguide (7), coupling mechanism (8, movement indicated by green arrows), and holder of the movable coupling piston (9). **(b–e)** $\boldsymbol{B}$ and $\boldsymbol{E}$ field simulations of the resonator with an empty quartz EPR tube ($\epsilon = 3.4$); isolines are spaced in 6 % steps of the maximum field strength with $z||B_0$ (see **a**); all cross sections run through the center of the cavity. **(b)** Strength of the x component of the B_1 field in a horizontal cross section. **(c)** Strength of the x component of the B_1 field in a vertical cross section. **(d)** Strength of the tangential E_1 field in a horizontal cross section. **(e)** Strength of the z component of the E_1 field in a vertical cross section.

heating and a reduction of the Q value due to lossy samples (Tschaggelar et al., 2009). Samples with a high dielectric constant focus the magnetic field B_1 in the center. This leads to an increase in the electric field E_1 at the sample borders, which induces a reduction in the Q value. This effect can also be seen when comparing microwave field simulations of the resonator with an EPR tube (Fig. 1) and without an EPR tube (Fig. S4), as well as in the increasing filling factor with increasing ϵ of the sample (Table S3). Whereas for an empty clear fused quartz tube the electric field penetrates only slightly into the interior of the tube, this penetration becomes stronger if the EPR tube is filled with a sample with a high dielectric constant such as liquid water. Particularly without an EPR tube, the electric field is not perfectly symmetric, as expected for a pure TE_{011} mode, but has a visible distortion due to a weak TE_{311} mode contribution (Figs. 1d and S4c). Mett and Hyde (2004) showed that these distortions can lead to microwave leakage through the modulation slots, thus reducing the resonator Q value; however, the low intensity of the second mode observed in the simulations suggests that the effect is minor in this case.

To map the sensitivity profile of the resonator as a guide for designing experiments, we probed the distribution of the magnetic component of the microwave field in the resonator and the shift of the resonance frequency upon sample insertion using a DPPH point sample with a defined EPR transition at $g = 2.0036$ (Eaton et al., 2010). The inserted sample was moved in steps of 1 mm from the bottom to the upper end of the resonator cavity. The frequency of the minimum of the reflection curve was measured with an external frequency counter as a function of the sample position (Fig. 2a). At each sample position, the spectrum of DPPH was measured, and the double-integral intensity was computed (Fig. 2b). Figure 2a shows that the measured and the predicted frequency shifts are in good agreement with each other for all sample positions. In Fig. 2b, the normalized double-integral intensity after linear baseline correction is shown in comparison with the B_1 field strength simulations. The measured CW EPR signal intensity of DPPH matches the one expected from simulations well. The experiment shows that the active height of the resonator is around 6 mm, which corresponds to an active sample volume of about 30 µL for a 3 mm OD sample tube; as expected, the maximum B_1 field is about 3–5 mm from the bottom, which corresponds to the center of the resonator.

To adjust the coupling for a range of samples with different dielectric constants, we tested a coupling element where the angle of the copper coupling rod with respect to the iris determines the coupling strength (Fig. 1a). The design allows for a broader range over which the coupling can be adjusted compared to the previous copper ring moving vertically in front of the iris on a PEEK rod (Tschaggelar et al., 2009). Therefore, the effect of the coupler tilt angle was investigated in more detail. Figure 3 displays the simulated and experimental microwave reflection curves for different positions of the coupling element. The coupling element was moved between -3 and $+3°$ around the resting position at 0° tilt angle. The frequency and Q value of the resonator are in quite reasonable agreement with the simulations, although some trends differ slightly. The slight deviation between the center frequency of the simulations and the experiment is most prob-

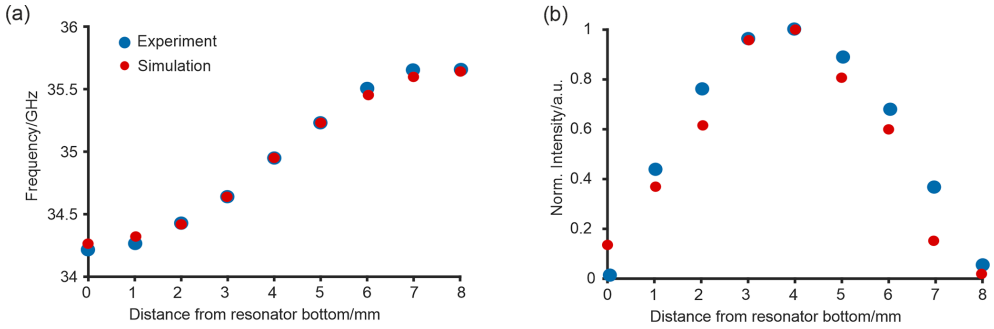

Figure 2. **(a)** Frequency of the resonator mode as a function of the position of a DPPH point sample (blue) and corresponding simulations (red). **(b)** Double-integral intensity of the corresponding DPPH sample at the same positions (blue) and the expected intensity from the simulations (red).

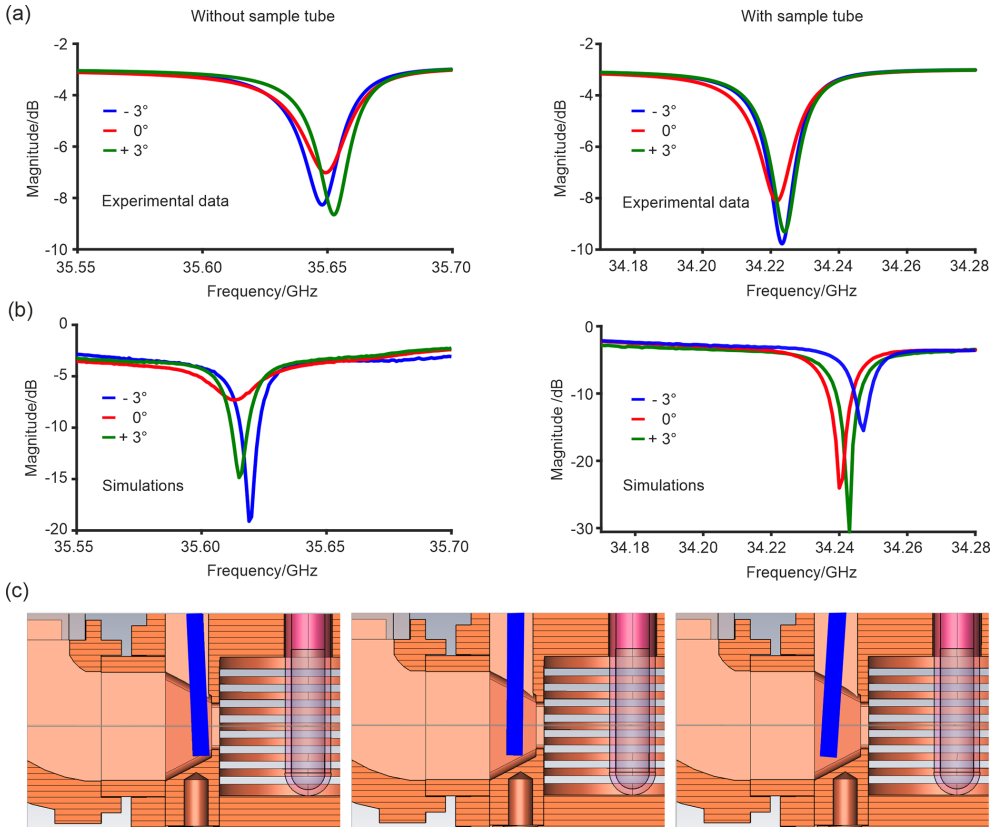

Figure 3. **(a)** Experimental frequency of the resonator mode as a function of the coupler position (tilt angle) without and with a clear fused quartz sample tube. No additional modes are observed in the range of 34–36 GHz. **(b)** The corresponding simulations with the same color code. **(c)** Positions of the coupler used for the simulation from left to right, -3 to $+3°$. The coupling element is highlighted in blue.

ably due to the non-perfect manufacturing of the surfaces, which leads to a decrease in the surface conductivity of the resonator material. Interestingly, the resonator features two very similar, distinct maxima in the Q value at a coupling rod angle of -3 and $+3°$. Since the magnitude of reflections at the dip center decreases (larger S_{11}) and the Q value decreases when the tilt angle gets smaller, the resonator must be in the overcoupled regime for all coupler positions (Table 1). The β coefficient calculated from the voltage standing wave ratio (VSWR) (see Table 1 and Sect. S1) underlines that the resonator is not fully critically coupled ($\beta \neq 1$), with or without the sample tube. Both experiments and simulations show a consistent increase in Q value for all coupler tilt angles upon inserting the quartz tube. This effect probably results from the tube acting as a dielectric ring that slightly pulls the electric field into the tube walls, as seen upon closer inspec-

tion of Figs. 1e and S4d. This, in turn, leads to a reduction in the electric field near the resonator walls. The coupler design tested here is, therefore, suitable for applications in CW EPR, although the coupling range is found to be less versatile compared to other published designs (Judd et al., 2022). Additional simulations (not shown) demonstrate that the observed broadband absorption of around 4 dB in all curves can be explained by the losses introduced by the top part of the waveguide made out of stainless steel, which is used to reduce the heat flow from the flange at room temperature to the cold resonator; these losses can be strongly alleviated by silver coating of the waveguide's inner walls (Tschaggelar et al., 2009; Himmler et al., 2022).

3.3 Microwave characteristics of the resonator

In order to assess the sensitivity of the EPR resonator, we quantify contributions to the EPR signal that characterize the resonator. The intensity of a CW EPR signal in the linear microwave power regime (no saturation) can be expressed as

$$S = \chi'' Q_{\mathrm{L}} \eta \sqrt{PZ}, \tag{1}$$

where S is the signal voltage at the end of the transmission line connected to the resonator, χ'' is the magnetic susceptibility of the sample, Q_{L} is the loaded quality factor of the resonator (see Eq. S2 in the Supplement), η is the filling factor as defined in Eq. (S5), P is the microwave power, and Z is the characteristic impedance of the transmission line (Eaton et al., 2010). Equation (1) shows that the signal-to-noise ratio can be optimized by increasing Q_{L} or η; both parameters are influenced by the sample tube diameter (Nesmelov et al., 2004). Here, the diameter was not varied to maximize the sensitivity for this resonator due to the design goal of using the same sample tube size in multiple resonators across the three frequency bands (S, X, Q), for which a diameter of 3 mm is a suitable common denominator.

The loaded Q value, Q_{L} (see Eq. S2), is a measure for the efficiency of the cavity (including the impedance matching (load) of the transmission line) in storing microwave energy versus dissipating energy, e.g., as ohmic losses. Accordingly, it can also be defined as the ratio between the energy stored in the resonator and the energy lost per cycle. The obtained Q_{L} value of 2550 (unloaded $Q_0 = 9475$; see Eq. S4) near critical coupling is on the higher end of previously reported values for home-built Q-band resonators based on the TE_{011} mode (see Table 2); similar values were obtained by resonators with oversized sample tube diameters, e.g., 2.8 mm OD with a Q_{L} value of 2480 by Judd et al. (2022) and 3.0 mm OD with a Q_{L} value of 2600 by Reijerse et al. (2012).

Although the introduction of an oversized lossy sample is expected to cause a reduction in the Q value, the overall sensitivity can still be higher due to the larger sample volume, which implies a larger number of spins at a given concentration (Tschaggelar et al., 2009). The increase in concentration sensitivity through the increased sample volume stems from a high filling factor η (defined in Eq. S5). Simulations show for the present Q-band TE_{011} resonator $\eta = 0.057$, with a 5 mm high sample in a 3 mm OD clear fused quartz tube, which is considerably higher than for a TE_{102} rectangular resonator with $\eta = 0.023$ (see Table 2). For both resonators, the filling factors increase for samples with higher dielectric constants due to an increased concentration of the microwave mode in the cavity center (Table S3). Comparing the two cavities, the TE_{011} resonator shows a significant improvement in η due to better focusing of the microwave B_1 field along the axis of the sample tube in the cylindrical cavity compared to the rectangular cavity. As a side effect, the resonance frequency of this high-η cavity is more susceptible to changes in the sample position compared to the TE_{102} resonator (Fig. 2a) because the sample diameter is of similar size as the wavelength, and a high proportion of the microwave field interacts with the sample (Fig. 1).

Ultimately, the signal intensity is driven by the strength of the B_1 field. The relation between the applied power (Eq. 1) and B_1 is defined as the conversion factor (C):

$$C = \frac{B_1}{\sqrt{P}}. \tag{2}$$

B_1 can be calculated from the length of a π pulse in a Rabi nutation experiment. For a γ-irradiated Herasil sample at room temperature and at 50 K, pulse nutation experiments show π pulse lengths of 46 and 44 ns (Fig. S5), corresponding to conversion factors of 0.45 and 0.52 mT $\sqrt{W}^{-1}$, respectively, similarly to previously published resonators (see Table 2). These experimental values are in good agreement with the calculated conversion factor of 0.55 mT $\sqrt{W}^{-1}$, determined from the simulated magnetic field strength in the center of the cavity with an empty 3 mm quartz tube. The nutation experiments further show that the resonator is also suitable for single-frequency pulsed EPR experiments. However, given the elevated Q value of the resonator, it is advantageous to use low-power and more selective pulses when a shorter spectrometer dead time is required.

3.4 CW EPR performance of the resonator

To demonstrate the sensitivity and spectral resolution of the Q-band resonator on relevant systems for current research applications, we measured room-temperature and low-temperature (30 K) CW EPR spectra of a homogeneous Ti(III) catalyst in toluene (Fig. 4). The Q-band CW EPR spectrum is an important complement to S-band and X-band spectra to resolve the different overlapping Ti(III) species present in this system with only slightly different g-tensor values. In the room-temperature Q-band CW EPR spectrum (Fig. 4b), three major components could be readily identified. In the low-temperature spectrum, in the absence of motional averaging, the full g anisotropy of the different components is observed. As discussed above, for echo-detected

Table 1. Microwave characteristics of the resonator. Experimental and simulated resonator mode for different coupler positions (tilt angle) with and without an empty 3 mm OD clear fused quartz tube. BW is bandwidth.

		Without sample tube				With sample tube			
	Position	ν_{dip} (GHz)	BW (MHz)	Q_L	β	ν_{dip} (GHz)	BW (MHz)	Q_L	β
Experiment	−3°	35.648	24.5	1455	3.39	34.223	13.4	2554	2.71
	0°	35.650	28.5	1251	4.41	34.222	16.4	2087	3.53
	+3°	35.653	21.5	1658	3.17	34.224	13.6	2517	2.89
Simulation	−3°	35.619	19.0	1875	1.35	34.247	15.0	2283	1.55
	0°	35.613	51.0	699	3.61	34.240	19.0	1802	1.17
	+3°	35.615	21.0	1696	1.61	34.243	18.0	1902	1.08

Table 2. Comparison of microwave characteristics with resonators from the literature.

Resonator type	Q_L	η^c	C in mT $\sqrt{W}^{-1}$	Tube diameter	Reference
TE_{011}	2080–2550	0.057	0.45–0.52	3 mm	This work
TE_{011}	450–950	n.d.	0.009	4 mm	Gromov et al. (2006)
TE_{011}	1300–2600[a]	n.d.	0.45	3 mm	Reijerse et al. (2012)
TE_{102}	200–400[a]	0.023	0.11	2.9 mm	Tschaggelar et al. (2009)
Loop gap[b]	250–700	n.d.	0.39–1.7	0.4–1.6 mm	Forrer et al. (2008)

[a] Empty 3 mm tube; n.d. stands for not determined. Ranges of Q_L values span the range from overcoupled to critically coupled. [b] Ranges are over several overcoupled three-loop, two-gap resonators. Note that Q_L and the conversion factor also depend on dielectric losses in a particular sample. [c] Note that higher η values are found for samples with $\epsilon > 1$ (see Table S3).

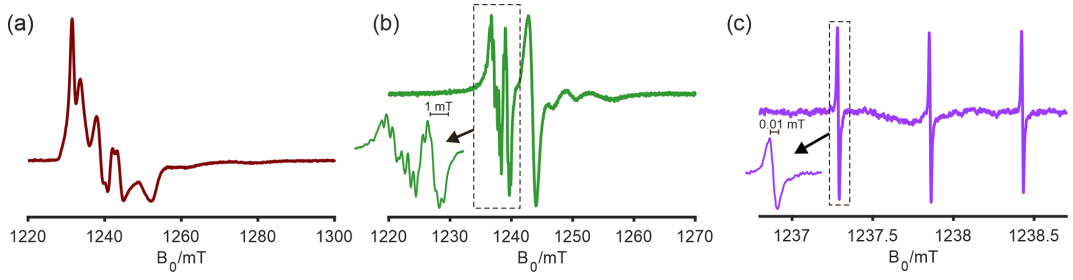

Figure 4. Q-band CW EPR spectra of a multi-component Ti(III)-complex system in toluene at 30 K **(a)** and at room temperature **(b)** and spectrum of 10 ppm N@C_{60} spin-diluted in C_{60} at room temperature **(c)**. The latter was measured on an extended powder sample (ca. 8 mm) with a modulation amplitude of 2 µT and shows a line width of 10 µT.

field-swept EPR spectra, the potential dependence of relative signal intensities on the magnetic field complicates global fitting with spectra in other frequency bands and hence hampers a quantitative analysis. In the case at hand, with the two Q-band CW EPR spectra, the g tensors of the three main components become sufficiently constrained. Together with the hyperfine couplings to surrounding nuclei, which are more clearly visible in the lower-frequency spectra, we established multi-frequency CW EPR analysis in the S, X, and Q bands on the same sample tube as an essential step to deconvolute overlapping spectral components and to understand the catalytic mechanism of this class of systems.

The resonator was also tested with spin-diluted N@C_{60}, as shown in Fig. 4c. In this sample, atomic nitrogen ($S = 3/2$, $I = 1$) is trapped in the center of the fullerene C_{60}, which renders the g tensor and the hyperfine coupling to the nitrogen very isotropic (Almeida Murphy et al., 1996; Weidinger et al., 1998; Wittmann et al., 2018). In the room-temperature Q-band CW EPR spectrum recorded with a single scan, one can observe three lines due to the ^{14}N hyperfine coupling, with each of the lines having a peak-to-peak line width of 0.01 mT. The spectra of the Ti(III) catalyst and N@C_{60} samples demonstrate the suitability of the resonator for applications from cryogenic to room temperature for samples with narrow and broad lines. Furthermore, a power saturation curve of TEMPOL radicals (100 µM, 20 µL) in frozen toluene solution demonstrates the onset and progressive saturation of the sample and shows a signal-to-noise ratio of 235 in a single scan (Fig. S6).

4 Conclusions

In this work, we introduced the design and fabrication of a 35 GHz cavity resonator for oversized samples and evaluated its performance in CW EPR and low-power pulsed EPR. The cylindrical resonator employs the TE_{011} mode and features a high filling factor of $\eta = 0.057$ that increases for high-dielectric samples and a high loaded Q value of around 2550 when near critical coupling or shows an overcoupled bandwidth of about 25 MHz with a 3 mm OD clear fused quartz tube. Electromagnetic field calculations are in good agreement with the experiments, highlighting the importance of rational resonator design and simulations as tools for geometry optimization. For the resonator, a high resolution was demonstrated with a linewidth of 10 µT for $N@C_{60}$. A Ti(III) catalyst with multiple spectral species was employed to demonstrate the general applicability of the probe head and its operation at cryogenic temperatures, as well as the benefit of resolving spectral overlap in complex systems. This resonator is, therefore, well-suited for CW EPR and also for single-frequency pulsed EPR experiments. Since the construction of the resonator is straightforward due to its simplistic and robust design, we hope that it will be leveraged to enhance the use of the Q band in multi-frequency EPR analyses.

Data availability. Design 3D CAD data are made available via Zenodo with https://doi.org/10.5281/zenodo.11082486 (Fischer et al., 2024).

Supplement. The supplement related to this article is available online at: https://doi.org/10.5194/mr-5-143-2024-supplement.

Author contributions. DK conceived the project and data processing. JS and JWAF performed the experimental work and data processing. RT and DK designed the resonator. RT performed the simulations analyzed by RT and DK. OO fabricated the resonator. NA, ABB, MI, and KM provided relevant test samples. JS, JWAF, RT, and DK wrote the paper with inputs from all authors. All authors discussed the results and contributed to the final paper.

Competing interests. The contact author has declared that none of the authors has any competing interests.

Disclaimer. Publisher's note: Copernicus Publications remains neutral with regard to jurisdictional claims made in the text, published maps, institutional affiliations, or any other geographical representation in this paper. While Copernicus Publications makes every effort to include appropriate place names, the final responsibility lies with the authors.

Financial support. This research has been supported by the ETH research grant (no. ETH-35221) to Daniel Klose and the SNSF grant (no. 200021_201070/1) to Alexander Benjamin Barnes.

Review statement. This paper was edited by Daniella Goldfarb and reviewed by two anonymous referees.

References

Almeida Murphy, T., Pawlik, T., Weidinger, A., Höhne, M., Alcala, R., and Spaeth, J.-M.: Observation of Atomlike Nitrogen-Implanted Solid C60, Phys. Rev. Lett., 77, 1075–1078, https://doi.org/10.1103/PhysRevLett.77.1075, 1996.

Bonke, S. A., Risse, T., Schnegg, A., and Brückner, A.: In situ electron paramagnetic resonance spectroscopy for catalysis, Nature Reviews Methods Primers, 1, 33, https://doi.org/10.1038/s43586-021-00031-4, 2021.

Denysenkov, V., van Os, P., and Prisner, T. F.: Q-Band Loop-Gap Resonator for EPR Applications with Broadband-Shaped Pulses, Appl. Magn. Reson., 48, 1263–1272, https://doi.org/10.1007/s00723-017-0930-9, 2017.

Eaton, G. R., Eaton, S. S., Barr, D. P., and Weber, R. T.: Quantitative EPR, Springer Vienna, ISBN 9783211929483, https://doi.org/10.1007/978-3-211-92948-3, 2010.

Eckardt, M., Wieczorek, R., and Harneit, W.: Stability of C60 and N@C60 under thermal and optical exposure, Carbon, 95, 601–607, https://doi.org/10.1016/j.carbon.2015.08.073, 2015.

Fischer, J. W. A., Stropp, J., Tschaggelar, R., Oberhänsli, O., Alaniva, N., Inoue, M., Mashima, K., Barnes, A. B., Jeschke, G., and Klose, D.: Design 3D CAD data of an oversized-sample 35 GHz EPR resonator with an elevated Q value, Zenodo [data set], https://doi.org/10.5281/zenodo.11082486, 2024.

Forrer, J., García-Rubio, I., Schuhmam, R., Tschaggelar, R., and Harmer, J.: Cryogenic Q-band (35GHz) probehead featuring large excitation microwave fields for pulse and continuous wave electron paramagnetic resonance spectroscopy: Performance and applications, J. Magn. Reson., 190, 280–291, https://doi.org/10.1016/j.jmr.2007.11.009, 2008.

Franco, L., Ceola, S., Corvaja, C., Bolzonella, S., Harneit, W., and Maggini, M.: Synthesis and magnetic properties of N@C60 derivatives, Chem. Phys. Lett., 422, 100–105, https://doi.org/10.1016/j.cplett.2006.02.046, 2006.

Froncisz, W. and Hyde, J. S.: The loop-gap resonator: a new microwave lumped circuit ESR sample structure, J. Magn. Reson., 47, 515–521, https://doi.org/10.1016/0022-2364(82)90221-9, 1982.

Gromov, I., Shane, J., Forrer, J., Rakhmatoullin, R., Rozentzwaig, Y., and Schweiger, A.: A Q-Band Pulse EPR/ENDOR Spectrometer and the Implementation of Advanced One- and Two-Dimensional Pulse EPR Methodology, J. Magn. Reson., 149, 196–203, https://doi.org/10.1006/jmre.2001.2298, 2001.

Gromov, I., Forrer, J., and Schweiger, A.: Probehead operating at 35GHz for continuous wave and pulse electron paramagnetic resonance applications, Rev. Sci. Instrum., 77, 064704, https://doi.org/10.1063/1.2216849, 2006.

Himmler, A., Albannay, M. M., von Witte, G., Kozerke, S., and Ernst, M.: Electroplated waveguides to enhance DNP and EPR

spectra of silicon and diamond particles, Magn. Reson., 3, 203–209, https://doi.org/10.5194/mr-3-203-2022, 2022.

Jakes, P., Dinse, K.-P., Meyer, C., Harneit, W., and Weidinger, A.: Purification and optical spectroscopy of N@C60, Phys. Chem. Chem. Phys., 5, 4080, https://doi.org/10.1039/b308284a, 2003.

Judd, M., Jolley, G., Suter, D., Cox, N., and Savitsky, A.: Dielectric Coupler for General Purpose Q-Band EPR Cavity, Appl. Magn. Reson., 53, 963–977, https://doi.org/10.1007/s00723-021-01404-4, 2022.

Matzler, C. and Wegmuller, U.: Dielectric properties of freshwater ice at microwave frequencies, J. Phys. D Appl. Phys., 20, 1623, https://doi.org/10.1088/0022-3727/20/12/013, 1987.

Mett, R. R. and Hyde, J. S.: Microwave leakage from field modulation slots in TE011 electron paramagnetic resonance cavities, Rev. Sci. Instrum., 76, 014702, https://doi.org/10.1063/1.1823748, 2004.

Mett, R. R., Sidabras, J. W., and Hyde, J. S.: Coupling of waveguide and resonator by inductive and capacitive irises for EPR spectroscopy, Appl. Magn. Reson., 35, 285–318, https://doi.org/10.1007/s00723-008-0162-0, 2009.

Misra, M.: Multifrequency Electron Paramagnetic Resonance: Theory and Applications, Wiley, ISBN 9783527633531, https://doi.org/10.1002/9783527633531, 2011.

NejatyJahromy, Y., Roy, S. C., Glaum, R., and Schiemann, O.: Multi-Frequency and Single-Crystal EPR on V4+ in W-Doped β-Vanadyl(V) Phosphate: Hyperfine Coupling- and g-Tensor Values and Orientation, Appl. Magn. Reson., 52, 169–175, https://doi.org/10.1007/s00723-020-01303-0, 2021.

Nesmelov, Y. E., Gopinath, A., and Thomas, D. D.: Aqueous sample in an EPR cavity: sensitivity considerations, J. Magn. Reson., 167, 138–146, https://doi.org/10.1016/j.jmr.2003.12.005, 2004.

Polyhach, Y., Bordignon, E., Tschaggelar, R., Gandra, S., Godt, A., and Jeschke, G.: High sensitivity and versatility of the DEER experiment on nitroxide radical pairs at Q-band frequencies, Phys. Chem. Chem. Phys., 14, 10762, https://doi.org/10.1039/c2cp41520h, 2012.

Raitsimring, A., Astashkin, A., Enemark, J. H., Blank, A., Twig, Y., Song, Y., and Meade, T. J.: Dielectric Resonator for K_a-Band Pulsed EPR Measurements at Cryogenic Temperatures: Probehead Construction and Applications, Appl. Magn. Reson., 42, 441–452, https://doi.org/10.1007/s00723-012-0313-1, 2012.

Reijerse, E. and Savitsky, A.: Electron Paramagnetic Resonance Instrumentation, eMagRes, 6, 187–206, https://doi.org/10.1002/9780470034590.emrstm1511, 2017.

Reijerse, E., Lendzian, F., Isaacson, R., and Lubitz, W.: A tunable general purpose Q-band resonator for CW and pulse EPR/ENDOR experiments with large sample access and optical excitation, J. Magn. Reson., 214, 237–243, https://doi.org/10.1016/j.jmr.2011.11.011, 2012.

Roessler, M. M. and Salvadori, E.: Principles and applications of EPR spectroscopy in the chemical sciences, Chem. Soc. Rev., 47, 2534–2553, https://doi.org/10.1039/c6cs00565a, 2018.

Savitsky, A., Grishin, Y., Rakhmatullin, R., Reijerse, E., and Lubitz, W.: An improved coupling design for high-frequency TE011 electron paramagnetic resonance cavities, Rev. Sci. Instrum., 84, 014704, https://doi.org/10.1063/1.4788735, 2013.

Schweiger, A. and Jeschke, G.: Principles of Pulse Electron Paramagnetic Resonance, Oxford University Press, ISBN 9780198506348, https://doi.org/10.1093/oso/9780198506348.001.0001, 2001.

Sidabras, J. W., Richie, J. E., and Hyde, J. S.: Axially uniform magnetic field-modulation excitation for electron paramagnetic resonance in rectangular and cylindrical cavities by slot cutting, J. Magn. Reson., 274, 115–124, https://doi.org/10.1016/j.jmr.2016.11.014, 2017.

Sienkiewicz, A., Smith, B. G., Veselov, A., and Scholes, C. P.: Tunable Q-band resonator for low temperature electron paramagnetic resonance/electron nuclear double resonance measurements, Rev. Sci. Instrum., 67, 2134–2138, https://doi.org/10.1063/1.1147027, 1996.

Stoll, S. and Schweiger, A.: EasySpin, a comprehensive software package for spectral simulation and analysis in EPR, J. Magn. Reson., 178, 42–55, https://doi.org/10.1016/j.jmr.2005.08.013, 2006.

Tschaggelar, R., Kasumaj, B., Santangelo, M. G., Forrer, J., Leger, P., Dube, H., Diederich, F., Harmer, J., Schuhmann, R., García-Rubio, I., and Jeschke, G.: Cryogenic 35GHz pulse ENDOR probehead accommodating large sample sizes: Performance and applications, J. Magn. Reson., 200, 81–87, https://doi.org/10.1016/j.jmr.2009.06.007, 2009.

Tschaggelar, R., Breitgoff, F. D., Oberhänsli, O., Qi, M., Godt, A., and Jeschke, G.: High-Bandwidth Q-Band EPR Resonators, Appl. Magn. Reson., 48, 1273–1300, https://doi.org/10.1007/s00723-017-0956-z, 2017.

Weidinger, A., Waiblinger, M., Pietzak, B., and Almeida Murphy, T.: Atomic nitrogen in C60:N@C60, Appl. Phys. A-Mater., 66, 287–292, https://doi.org/10.1007/s003390050668, 1998.

Wittmann, J., Can, T., Eckardt, M., Harneit, W., Griffin, R., and Corzilius, B.: High-precision measurement of the electron spin g factor of trapped atomic nitrogen in the endohedral fullerene N@C60, J. Magn. Reson., 290, 12–17, https://doi.org/10.1016/j.jmr.2018.02.019, 2018.

Zhang, Z., Fleissner, M. R., Tipikin, D. S., Liang, Z., Moscicki, J. K., Earle, K. A., Hubbell, W. L., and Freed, J. H.: Multifrequency Electron Spin Resonance Study of the Dynamics of Spin Labeled T4 Lysozyme, J. Phys. Chem. B, 114, 5503–5521, https://doi.org/10.1021/jp910606h, 2010.